Maximum Effectiveness of Electrostatic Energy Harvesters When Coupled to Interface Circuits

Paul D. Mitcheson, *Senior Member, IEEE*, and Tim C. Green, *Senior Member, IEEE*

***Abstract*—Many motion driven energy harvesting devices using the electrostatic force have been demonstrated, with many of them using a moving plate, variable capacitor structure. The output power of all reported electrostatic energy harvester systems that interface to an energy storage element is at least one and sometimes more than two orders of magnitude below the theoretical maximum limit for the given device dimensions and driving motion. This paper shows that the theoretical limits on the harvester performance when only the coupling effectiveness is considered are misleading and that when the transducer and its power processor interface are combined, further important limitations apply which significantly reduce the theoretical maximum power. The combined analysis rests on a parameterization of the inherent and parasitic properties of key components, notably the power semiconductor devices. Although scaling laws in general favour electrostatic force solutions over electromagnetic force solutions at micro scale, the specific compromises encountered with the interface circuits for electrostatic generators means that their range of applications needs to be re-examined.**

Under previous analysis, the choice of constant charge or constant voltage operation has not been fully resolved. The new analysis shows that when the power electronic interface is considered together with the transducer, the performance of the constant charge harvester system is generally poor, although an acceptable region of operation limited to intermediate sizes and accelerations exists. The constant voltage device can operate with acceptable effectiveness over a much wider envelope, and is thus the preferred implementation. The optimization of the transducer and interface circuits underlying these conclusions was performed in MATLAB and verified with time-domain PSpice simulations.

***Index Terms*—Energy harvesting, electrostatic transducer, vibration-to-electric energy conversion**

I. Introduction

ENERGY harvesting micropower generators use either the electromagnetic [1] or electrostatic [2] forces to convert kinetic energy into an electrical form. Electrostatic devices have been demonstrated using capacitor structures with moving electrodes [3], [4], piezoelectric materials [5] and electrorestrictive polymers [6]. Electromagnetic devices have been demonstrated using conventional permanent magnets and coils [7] and with magnetorestrictive materials [8]. Each transduction mechanism has relative advantages and disadvantages but the debate as to which method is superior is still unanswered. The argument in favour of moving electrode electrostatic devices centres on the superiority of the scaling of the electrostatic force at the microscale [9] and better compatibility with semiconductor processing. In this paper we perform a complete analysis of moving electrode electrostatic energy harvesters, including the necessary power processing interface to a storage battery or capacitor, to determine for the first time the limits on performance of this transducer when used in a complete energy harvesting system. The equations are parametrised in a way which allows the performance limits of these systems to be determined as a function of their size and the amplitude and frequency of the driving motion.

Earlier work into finding the best choice of transducer for an energy harvester under different operating conditions was presented in [10]. However, in that paper the assumption was made that each harvester was dissipating energy into an optimised resistive load. This is a simplification which does not take into account the requirements of interfacing the transducer with low power electronics and energy storage and hence only determines the limits on the transducer in isolation. In [11], the performance of a constant charge mode generator is discussed in terms of the parasitic loading and voltage limitations brought about by the interface circuit. However, the analysis of the circuit efficiency is not included. Here, we find the upper limit on the end-to-end harvester performance when the energy storage and interface electronics are considered as part of the system. This is achieved by building a coupled model which includes the mechanical elements, the electrostatic transduction and the interface circuit (which in turn includes detailed semiconductor models).

We show that, whilst the electrostatic force may be the superior force at the microscale when used for actuation purposes [12], electrostatic devices can behave poorly when used as generators. This is because for a MEMS actuator, the primary design concern is maximising output force or mechanical output power whereas, for a generator, the efficiency of the power conversion is the main concern. The difficulties arise because the extreme combinations of low charge and high voltage required to optimise the transducer coupling effectiveness place requirements on the power electronics which are very difficult to achieve [13]. The coupling effectiveness alone is therefore a misleading metric when considering the performance of energy harvesting systems. To demonstrate that this low efficiency is an inherent feature of electrostatic generators and not merely the result of non-optimal design requires a complete model of the the transducer plus a power processor system which has been parameterized (in terms of core components and unavoidable parasitic effects) in such a way that optimal designs and corresponding efficiencies can be identified as a function of scale. Here, we use such a model to determine combinations of generator size and acceleration for which an electrostatic harvester system can operate effectively, giving equations for suitable regions of operation.

Paul D. Mitcheson and Tim C. Green are with the Department of Electrical and Electronic Engineering, Imperial College London, London, UK, e-mail: paul.mitcheson@imperial.ac.uk.

Manuscript received Dec. 2011; revised May 2012; accepted May 2012

Copyright ©2012 IEEE. Personal use of this material is permitted. However, permission to use this material for any other purposes must be obtained from the IEEE by sending an email to pubs-permissions@ieee.org.

A. Methodology

In the analysis presented here, the end-to-end system effectiveness of switched constant voltage and constant charge electrostatic energy-harvesters [2] is considered as a function of their size and driving vibration characteristics when connected to a power conditioner. Continuous-type electrostatic systems using moving electrode capacitors such as those proposed in [14], [15] are not considered as they dissipate energy into a resistor rather than storing it in a battery or capacitor. When such systems are attached to a rectifier and energy storage element they typically become switched constant voltage harvesters [16]. Energy harvesters which use active materials as the transduction mechanism, such as piezoelectrics and electrorestrictive polymers are not considered here because the manufacturing processes, method of operation and power processing requirements for such systems are very different to those for moving electrode capacitor devices. Electromagnetic harvesters are not considered for the same reason.

In this work, the power conditioning circuits are chosen to be as simple as possible whilst still maintaining the minimum functionality to be able to operate the electrostatic transducer in an optimal way and to extract the generated electrical energy into a storage element, *e.g.* a battery or super-capacitor. Two circuit topologies are evaluated: one for the constant charge mode of operation and one for constant voltage mode. Circuit topologies other than the ones analysed here are possible, *e.g.* [17], and whilst the general trends in harvester performance are likely to be common across other circuit types, the specific performance figures will differ between different circuit topologies.

The rest of this paper is organised as follows. Background material is presented on the mechanical system, performance metrics and the transducer and circuit configurations. Next, key expressions regarding system performance are derived in terms of the parameters of generator size and input excitation amplitude and frequency. The optimisation of the system using the coupled electro-mechanical models is then described. Results for the performance of both the constant voltage and constant charge generators are then discussed and compared.

II. Background

An overview of the harvester's mechanical system, transducer topology and operation, along with the basic power processing circuits will now be described along with the performance metrics which are used to quantify generator performance. A more detailed discussion of these metrics can be found in [18].

A. Mechanical System

The now standard mechanical model of a vibration-driven energy harvester is that of a mass-spring-damper system whose internal components have a limited travel range due to the finite size of the device. In this model, the damper represents the transduction mechanism and its mechanical-domain velocity-force characteristic is dependent on the implementation of the transducer. Whilst it is possible with sufficiently advanced electronics to create any type of velocity-force characteristic with the electrostatic transduction mechanism, the most suited and widely adopted damper type is the Coulomb damper, [19]. A mechanical system model of an energy harvester with a Coulomb damper is shown in Fig. 1.

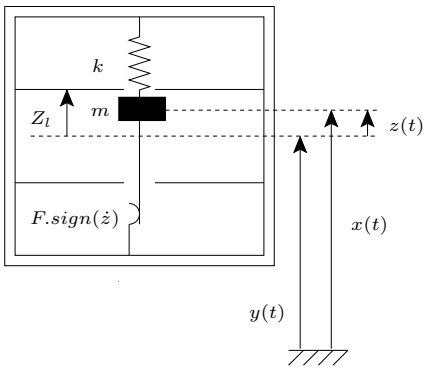


Fig. 1. Model of Coulomb-damped resonant generator (CDRG).

In [19], different types of generator were analysed and two architectures of electrostatic microgenerator implementations were discussed, these being the Coulomb-damped resonant generator (CDRG) and the Coulomb-force parametric generator (CFPG). The diagram of Fig. 1 is an implementation of a CDRG (becoming a CFPG when the spring constant, k, tends to zero). As only one prototype electrostatic CFPG has been demonstrated [3], the far more common CDRG device type is used in this paper as the model for the mechanical system.

Some additional assumptions are made here with regard to the mechanical set-up in order to bound the analysis. The generator is assumed to be cube shaped with length l (see [20] for a discussion on how generator aspect ratio effects performance), the proof mass is assumed to be made of gold (a dense MEMS compatible material) and to occupy half of the generator volume (optimal for resonant operation [19]) and the the spring suspension is assumed to occupy a small volume inside the generator frame (as is the case for previously reported electrostatic devices such as [3], [4], [15], [21]). The space occupied by the variable capacitance transduction mechanism is accounted for in the analysis and is discussed in more detail in SubSecs. III-A and III-B.

A part of the system volume must also be allocated to the interface circuit and it is assumed that the circuit occupies an additional volume equal to that swept out by the harvester's proof mass (*i.e.* the circuit occupies an additional volume of l^3). The allocated circuit volume is then apportioned equally between the inductors present in the system, with the semiconductor components (diodes and transistors) themselves assumed to consume negligible space. Energy storage in the form of a battery or capacitor is not assumed to be part of the system volume as this does not effect power density and is application specific and sized depending on the load duty cycle and the source intermittency characteristics.

B. Effectiveness and Efficiency

The effectiveness of an energy harvester system, η_{system}, is the product of two terms, coupling effectiveness, $\eta_{coupling}$, and

conversion efficiency, η_{conv} [18], [19]. Coupling effectiveness is a measure of the amount of work done against the damper per cycle, $E_{coupled}$, as a fraction of the maximum possible energy, the opportunity energy E_{opp}, that could have been coupled if the generator was optimally configured and all components were ideal. E_{opp} is the ultimate limit on the total energy per cycle that can be harvested for a given volume of inertial generator under a given mechanical excitation. The conversion efficiency is the energy extracted from the transducer into a useful form, E_{out}, as a fraction of the total coupled energy, $E_{coupled}$. Thus it measures the efficiency of the energy extraction electronics in transferring energy from transducer to an electrical energy storage device. Changes to the design of the generator and power electronic interface which increase $\eta_{coupling}$ may decrease η_{conv} [13] and so it is important that a maximum of the product is found rather than maximising the individual terms in isolation. The overall system effectiveness (which has a maximum value of 1) can therefore be written as:

$$\eta_{system} = \frac{E_{out}}{E_{opp}} \quad (1)$$

$$= \eta_{coupling} \times \eta_{conv} = \frac{E_{coupled}}{E_{opp}} \times \frac{E_{out}}{E_{coupled}} \quad (2)$$

In order to maximise $\eta_{coupling}$ for the simple mechanical model of the CDRG as shown in Fig. 1, an optimal damping force F_{opt} should be chosen. This is the force which allows maximum power to be dissipated in the damper during steady state mechanical excitation of the harvester and, for the system of Fig. 1, the work done by this force represents the ultimate limit of energy conversion from a kinetic to electrical form. Assuming parasitic damping is negligible due to the use of vacuum packaging (250 Pa has been demonstrated for electrostatic harvesters [22] and under 1 Pa has been obtained for MEMS resonators [23]), the optimal displacement constrained Coulomb damping force, $F_{opt_{CZ}}$, is given in [19] as:

$$F_{opt_{CZ}} = \frac{mY_0\omega^2\omega_c}{|U|}\sqrt{\frac{1}{\left(1-{\omega_c}^2\right)^2} - \frac{1}{{\omega_c}^4}\left(\frac{Z_l}{Y_0}\right)^2} \quad (3)$$

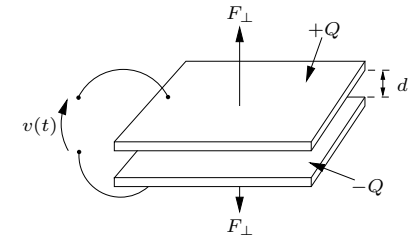
where $U = \frac{\sin(\frac{\pi}{\omega_c})}{1+\cos(\frac{\pi}{\omega_c})}$, ω is the angular frequency of the driving acceleration, ω_c is the operating frequency divided by the system resonant frequency, Y_0 is the amplitude of the driving motion, m is the value of the proof mass and Z_l is the maximum internal travel amplitude of the mass.

At resonance ω_c=1 and the value of (3) is undefined. Therefore the value of $F_{opt_{CZ}}$ to use at or close to resonance must be found by calculating the limit of (3) as $\omega_c \rightarrow 1$, as in [24], giving:

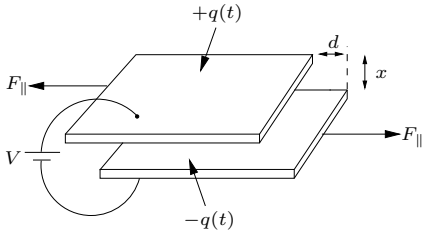
$$F_{opt_{CZres}} = \frac{\pi}{4}mA_0 \quad (4)$$

where A_0 is the peak input acceleration equal to $Y_0\omega^2$. Note that the stick-slip motion that can occur with a coulomb damped system [19] does not occur when the device is operated at resonance. For optimal device operation, therefore, the aim is to configure the electrostatic damper by setting the voltage or charge on the electrodes to provide a damping force equal to that defined by (4) in order to maximise $\eta_{coupling}$. The energy should then be extracted from the capacitor through the use of an efficient power electronic interface in order to maximise η_{conv}. In a few reported examples of electrostatic devices which were tested with a power electronic interface, many have had moderate values of η_{conv} at the expense of very low values of $\eta_{coupling}$ [25], [26]. In this paper we determine the maximum value of the product of those two terms.

C. Capacitor Configurations



(a) Constant charge



(b) Constant voltage

Fig. 2. Two common configurations of the electrostatic transducer. Both configurations provide a Coulomb force characteristic.

Two configurations of capacitor are able to readily create a Coulomb force: a gap closing arrangement operated in constant charge mode or a sliding arrangement operated in constant voltage, with the latter being functionally equivalent to the standard MEMS comb-drive actuator. These arrangements are shown in Fig. 2. Operating the transducer in constant voltage or constant charge mode as the plates move relative to each other is considered attractive because this can be achieved ether by connecting the plates to a constant voltage source during the generation cycle or leaving them open circuit during that cycle, thus simplifying the power electronic interface to the transducer.

Meninger previously argued [27] that the constant voltage cycle is capable of generating more electrical energy than the constant charge cycle. This is true under some operating modes for a given design of capacitor and fixed maximum allowable capacitor voltage. However, the design of constant charge and constant voltage generators may differ in terms of the structure of the MEMS capacitor and the power electronics and therefore both types of system are fully evaluated here before reaching a conclusion as to which configuration is optimal.

1) Constant Charge Configuration: The QV generation cycle of an electrostatic transducer operating in constant charge mode is shown in Fig. 3 and a simple power electronic

interface capable of enabling this operation is shown in Fig. 4. The axes in Fig. 3 represent the charge on and voltage across the plates of the moving electrodes during the different stages of generator operation. The source, V_{supply}, in Fig. 4 is envisaged as a low voltage battery which acts as the energy storage element and also provides a stable DC rail voltage to any circuitry to be powered from the generator. It is therefore expected to be at a potential of a few volts. The operation of this system is as follows: the capacitor is pre-charged in the high capacitance position (A→B) to a voltage V_{pc} with a charge Q_{opp}. With the assumption that the required value of V_{pc} is greater than V_{supply} (reasonable given the low voltages of V_{supply} that are envisaged as supplies for wireless sensor nodes), this is done by pulsing MOSFET M_2 in Fig. 4 so that energy is moved from the battery to the variable capacitor through the drain body diode of M_1 (or alternatively M_1 can be used as a synchronous rectifier).

Next, the electrodes separate under constant charge (M_1 and M_2 remain off), reducing the capacitance and increasing the voltage across the electrodes to a value V_{max} (B→C). It is very important that the electrodes remain isolated during this part of the cycle so that charge sharing or leakage through M_1 is minimised (non-ideal MOSFET characteristics are indicated in Fig. 4) as this causes a reduction in generated energy. Finally the energy in the variable capacitor is transferred into the storage element by pulsing M_1, such that the interface circuit operates as a buck converter (C→A), with M_2 acting either as a passive diode or a synchronous rectifier.

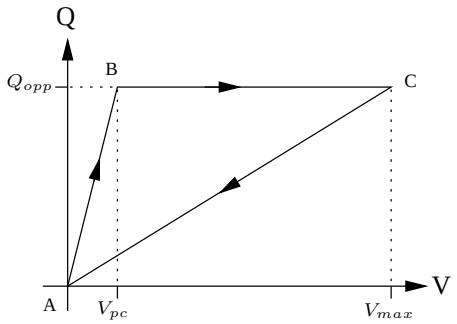


Fig. 3. Idealised charge versus voltage (QV) generation cycle for the operation of the variable capacitor in constant charge mode.

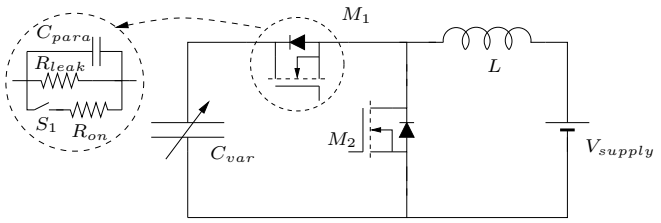


Fig. 4. Basic circuit for operation of constant charge mode generator, highlighting the non-ideal characteristics of the MOSFET switches.

2) Constant Voltage Mode: The constant voltage cycle is shown in Fig. 5 and a circuit for implementing the operation is shown in Fig. 6. Other circuit topologies have recently been presented, such as [28]. Unlike in the constant charge case, where a source of energy (the battery) is only required for priming the variable capacitor before the generation stroke, the constant voltage configuration requires a high voltage source to be placed in parallel with the variable capacitor during that stroke. Given that the required transducer operating voltage is likely to be significantly higher than the battery voltage, an intermediate high voltage stage is needed (C_{int} in Fig. 6) which can then be followed by an additional circuit to step-down the high voltage charge into a low voltage battery which powers the load. Prior to normal operation of the circuit of Fig. 6, the intermediate stage C_{int} is charged to the operating voltage V_{opp} by action of switches M_3 and M_4 acting as a boost converter, transferring energy from the battery to C_{int}.

After this priming of C_{int}, operation around the QV loop of Fig. 5 by the action of the circuit of Fig. 6 is as follows: during the generation cycle MOSFETS M_3 and M_4 remain off. The variable capacitor is first pre-charged (A→B) at maximum capacitance by pulsing M_1 and with M_2 acting passively or synchronously until the voltage on C_{var} is equal to V_{opp}. Next, the electrodes separate at constant voltage (B→C), during which time M_2 remains off and M_1 remains on, holding the voltage of the variable capacitor at the optimal voltage that maximises $\eta_{coupling}$. During this phase, charge is pushed off the moving electrodes, at constant voltage, into C_{int}, increasing the electrical energy stored. We assume that C_{int} is large enough that the change in its voltage is negligible during the generation stroke. Finally, the electrodes move back to their initial position under constant charge (M_1 and M_2 remain off) and the moving capacitor voltage reduces (C→A). During this operation, there should be very little residual charge, Q_{res}, on the electrodes as almost all of the charge should have been removed and pushed back into V_{supply} when the electrodes previously separated during (B→C). MOSFETS M_3 and M_4 and inductor L_2 then act as a buck converter arrangement for the transfer of the generated energy from the intermediate capacitance to the battery, V_{supply}.

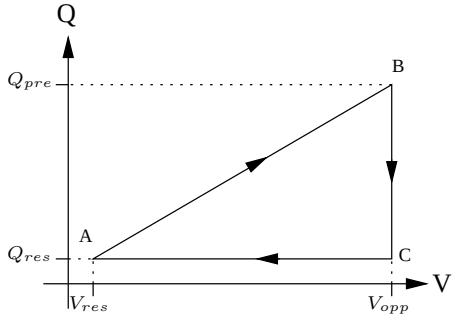


Fig. 5. Idealised charge versus voltage (QV) generation cycle the operation of the variable capacitor in constant voltage mode.

D. Model Parameterisation

The analysis presented in this paper relies on the paramaterisation of $\eta_{coupling}$ and η_{conv} into a common set of system input parameters, namely generator characteristic length l,

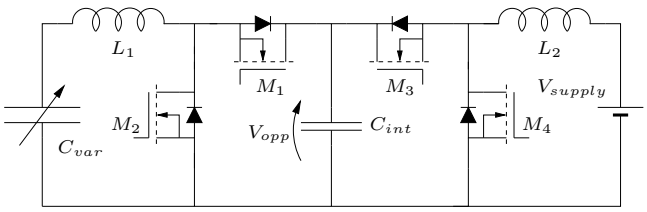


Fig. 6. Basic circuit for operation of constant voltage mode generator.

input acceleration magnitude A_0, operating frequency ω and one variable to be optimised: the cross-sectional area, A_{semi}, of the semiconductor devices in the interface circuits of Figs. 4 and 6. Once the relevant expressions have be written in terms of only these three known input parameters, physical constants and the unknown parameter A_{semi}, the coupled models can be constructed and solved to find the optimal value of A_{semi} which maximises η_{system}, thus allowing the performance limit of electrostatic harvesters to be found as a function of generator size and input excitation. This parameterization will now be performed for the relevant electromechanical properties of the constant charge generator, constant voltage generator, the semiconductor devices and the passive components.

III. Model Parameterisation: Transducers

A. Constant Charge Transducer

For the CDRG operating in constant charge mode, the system is assumed to be physically constructed in a way similar to the schematic configuration in Fig. 7. The moving mass, m is constrained to move within a cube with sides of length l and in an optimal configuration it occupies half of the volume of the cube [19]. The variable capacitance is formed between the lower side of the moving mass and electrode E_b when the mass moves upwards relative to the frame, and between the upper side of the moving mass and the electrode E_t when the mass moves in the opposite direction. As can be seen, the volume occupied by the transducer is negligible in this case as the dielectric volume naturally fits into the space required for the movement of the proof mass and the electrodes can be made very thin, thus occupying almost no volume.

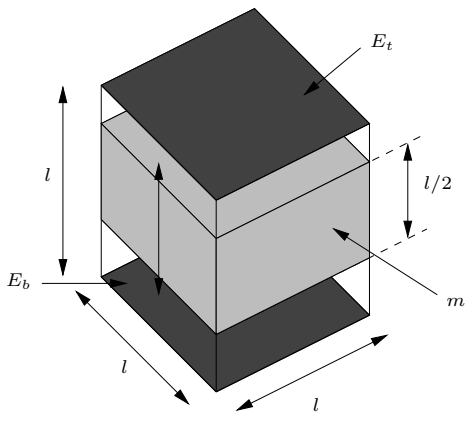


Fig. 7. Physical configuration of switched constant charge generator.

In constant charge operation, the force ($F_\perp$ in Fig. 2(a)) between the capacitor plates of area A_{plate} is independent of plate separation and can be controlled by setting the charge Q_{opp} on the plates according to:

$$F_\perp = \frac{1}{2}\frac{{Q_{opp}}^2}{\epsilon_0 A_{plate}} \tag{5}$$

where ϵ_0 is the permittivity of free space. Consequently, the charge on the capacitor of the constant charge generator should be chosen so that (5) is equal to the force which allows the maximum force to be converted from mechanical to electrical form, given by (4). This means that the optimal pre-charge voltage on the capacitor can be written as:

$$V_{pc_{opt}} = k_{v_{cq1}}(d_0)\sqrt{\frac{mY_0\omega^2}{A_{plate}}} \tag{6}$$

where $k_{v_{cq1}} = 4.21 \times 10^5$ V·s·kg$^{-1/2}$·m$^{-1/2}$ and d_0 is the initial separation between the electrodes, assumed here to be 10 μm. Given the assumptions on generator geometry (Fig. 7), and with a gold proof mass, this can be simplified to give:

$$V_{pc_{opt}} = k_{v_{cq2}} d_0 \sqrt{lA_0} \tag{7}$$

where $k_{v_{cq2}} = 4.14 \times 10^7$ V·s·m^{-2}, l is the length of a side of the generator and A_0 is the peak value of the driving acceleration. In constant charge operation, the electric field strength between the electrodes remains constant during separation (B→C in Fig. 3) and so the maximum voltage across the electrodes of the variable capacitor occurs when the electrode separation is maximum at the end of the generation stroke, giving:

$$V_{end_{opt}} = k_{v_{cq1}}(2Z_l)\sqrt{\frac{mY_0\omega^2}{A_{plate}}} \tag{8}$$

Again, assuming a gold proof mass with the geometry of Fig. 7, this can be simplified further to give:

$$V_{end_{opt}} = \frac{1}{2}k_{v_{cq2}}\sqrt{l^3A_0} \tag{9}$$

This equation therefore sets the maximum voltage which must be blocked by any semiconductor switches (M_1 and M_2 in Fig. 4) attached to the generator if the system is to operate with maximum power density, solely in terms of physical constants and optimisation input parameters A_0 and l.

B. Constant Voltage Transducer

For constant voltage mode, the generator is again assumed to be a cube with the generator taking the form of the schematic shown in Fig. 8. Two comb-drives are required in order to generate energy when the mass moves in either direction. The two comb-drives would probably be on the same sides of the cube but are shown here on adjacent sides for illustrative purposes. The comb electrodes on the moving mass (E_m) mesh alternately with the top (E_t) and bottom (E_b) electrodes, with E_m and E_t in operation when the mass moves away from E_t, and E_m and E_b in operation when the

mass moves in the opposite direction. As can be seen, the transducer in this case does consume some volume within the cubic package, with the amount consumed being proportional to the height of the comb-fingers. In the results presented in this paper, the reduction in the value of the proof mass due to the allocation of volume to the comb electrodes is included and reduces the maximum coupled power into the system, reducing $\eta_{coupling}$.

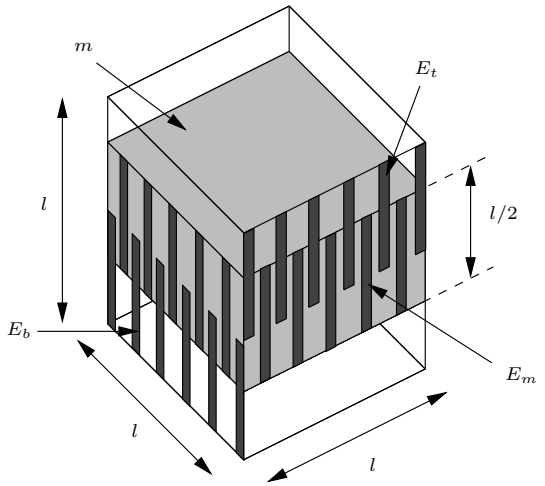


Fig. 8. Physical configuration of constant voltage mode generator.

For a comb drive, which exhibits a linear change in capacitance between C_{max} and C_{min} over a distance $2Z_l$ as required here, the electrostatic in plane sliding force ($F_{\parallel}$ in Fig. 2(b)) can be written as:

$$F_{\parallel} = \frac{1}{2}V^2\left(\frac{C_{max} - C_{min}}{2Z_l}\right) \tag{10}$$

where V is the voltage across the electrodes. Equating (10) with the force required to maximise $\eta_{coupling}$ (4), the optimal operating voltage for the constant voltage CDRG can be obtained as:

$$V_{opp_{opt}} = \sqrt{\frac{1.57mY_0\omega^2 2Z_l}{C_{max} - C_{min}}} \tag{11}$$

Again assuming a gold mass, cubic generator, negligable volume allocated to the transducer and suspension and that $C_{max} \gg C_{min}$, the expression for the optimal voltage can then be reduced to:

$$V_{opp_{opt}} = k_{v_{cv1}} l^2 \sqrt{\frac{A_0}{C_{max}}} \tag{12}$$

where $k_{v_{cv1}} = 87$ V·s·F$^{1/2}$·m$^{-5/2}$. In the results presented in this paper a size-dependent correction is applied to Eqn. 11 and hence Eqn. 12 to account for the proof mass reduction due to necessary volume allocated to the comb electrodes.

Unlike the constant charge configuration, where the maximum generator voltage corresponds to the minimum (electrodes open) capacitance which in turn is set purely by the size of the generator, in the constant voltage configuration the maximum voltage is set by C_{max} which is a technology dependent parameter. Assumptions on the limits of this technology must therefore be made with regard to the dimensions of the combs. Here, we assume that the achievable comb dimensions have an aspect ratio of 10:1 for a typical DRIE process where the comb width and height is 50 μm (*e.g.* see [29]), with a 5 μm gap. These assumptions are made because the dimensions of the device in [29] are 3×3 mm, which is approximately the centre point of generator size investigated in this paper. In the worst case (*i.e.* for the smallest generator considered here) the volume consumed by the comb drive transducer reduces the value of the proof mass by 25%, reducing the value of m in Eqn. 11 and in turn reducing the coupling effectiveness of the system.

Using the comb dimensions in [29], the maximum (closed position) comb drive capacitance can be written as a function of l, as:

$$C = k_{v_{cv2}} l^2 \tag{13}$$

where $k_{v_{cv2}} = 8.05 \times 10^{-7}$ F/m^2. This allows the optimal operating voltage to be written solely as a function of the variables l and A_0, as:

$$V_{opp_{opt}} = k_{v_{cv3}} l \sqrt{A_0} \tag{14}$$

where $k_{v_{cv3}} = 9.70 \times 10^4$ V·s·m$^{-3/2}$. This voltage is the maximum that M_1 to M_4 in Fig. 6 must be able to block in the off-state.

Having found the maximum values of moving electrode voltages that maximise $\eta_{coupling}$ for both constant charge and constant voltage mode operation as a function of microgenerator size l and acceleration amplitude A_0, the characteristics of the semiconductor devices, in terms of junction capacitance, on-state conduction loss and off-state leakage will now also be found as a function of these parameters.

IV. Model Parameterisation: Semiconductors and Passive Components

Real power electronic switches required by the interface circuit have finite off-state impedance, finite on-state conductance and contain depletion layer capacitances inherent in all *pn* blocking junctions. These non-idealities are indicated in Fig. 4 and they all cause reductions in η_{system} either by reducing the efficiency of the power processing circuits (and hence reducing η_{conv}) or by allowing charge leakage and charge sharing between the moving electrodes and the blocking junction (hence reducing $\eta_{coupling}$). The minimisation of these effects in a power MOSFET switch through the choice of optimised doping will now be briefly discussed in order to calculate the per-area values of junction capacitance, and on and off-state resistances of the semiconductor as a function of l and A_0.

The structure of the typical power MOSFET considered in this analysis is shown in Fig. 9. Although it has previously been shown that a minority carrier device may be beneficial for use in energy harvesting applications [30], for simplicity the MOSFET is the only controllable switch considered here. A minority carrier device may improve performance by up to 20% under some situations [30].

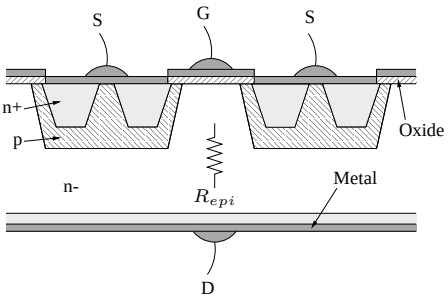


Fig. 9. Typical power MOSFET construction, showing the resistance of the *n-* epi region.

A. Device On-state Conduction Loss

For a given blocking voltage, it is advantageous to minimise the specific on resistance, *i.e.* the resistance of a unit area of device when switched on. This will allow conduction losses to be minimised for a given device area and thus the junction capacitance to be minimised for a given conduction loss. In high voltage MOSFETs, as will be required by typical electrostatic energy harvesters operating with an optimal electrostatic force [3], the dominant component of the drain-source resistance is the *n-* epi-layer, which must be long and relatively lightly doped in order to be able to support a high blocking voltage. Assuming that the epi-layer has uniform doping, the optimal doping density which minimises the specific on-state resistance of a silicon MOSFET is given in [31] as:

$$N_D = \frac{k_{N_D}}{V_B} \tag{15}$$

where V_B is the blocking voltage capability of the junction and $k_{N_D} = 14 \times 10^{22}$ V/m^3 [31]. When this optimal doping is used, the minimum resistance of the epi-layer of the MOSFET able to block a given voltage, V_B, is given in [31] as:

$$R_{epi} = \frac{k_{epi} {V_B}^2}{A_{semi}} \tag{16}$$

where $k_{epi} = 2 \times 10^{-11} \Omega$ m^2/V^2 and A_{semi} is the cross sectional area of the conducting epi-layer.

1) Constant Charge Mode Parameterisation: The minimised specific on resistance of the MOSFET can now be found for constant charge operation, by substituting the required blocking voltage (9) into (16), to give:

$$R_{epi_{cq}} = \frac{k_{epi} {k_{v_{cq2}}}^2 l^3 A_0}{4 A_{semi}} \tag{17}$$

2) Constant Voltage Mode Parameterisation: The equivalent expression for the constant voltage mode generator is found by substituting (14) into (16) to give:

$$R_{epi_{cv}} = \frac{k_{epi} {k_{v_{cv3}}}^2 l^2 A_0}{A_{semi}} \tag{18}$$

B. Device Junction Capacitance

Charge which is shared between the moving plate capacitor and any connected semiconductor will reduce the energy generated per stroke in the constant charge case and causes reverse recovery losses in both the constant charge and voltage modes. Therefore, the charge which is stored in the depletion capacitance of the device when in reverse bias must be determined. For the optimal doping concentration given in (15), the junction capacitance is given by:

$$C_j = \frac{A_j}{2} \sqrt{\frac{2 q \epsilon_0 \epsilon_r}{(V_0 - V_{operation})} N_D} \tag{19}$$

where A_j is the area of the junction, V_0 is the built in junction potential, $V_{operation}$ is the external junction bias voltage, N_D is the donor doping density in the *n-* region, q is the charge on the electron and ϵ_r is the relative permittivity of silicon. In the rest of this work, it is assumed that the junction area is approximately the same as the cross sectional area of the conducting epi-layer. Substituting the optimal doping value from (15) into (19) gives:

$$C_j = \frac{k_{cj} A_{semi}}{\sqrt{(V_0 - V_{operation}) V_B}} \tag{20}$$

where $k_{cj} = 1.1 \times 10^{-3}$ C/m^2.

1) Constant Charge Mode Parameterisation: The junction capacitance for the constant charge mode generator can then be found in terms of l and A_0 by substituting (9) into (20), to give:

$$C_{j_{cq}} = k_{cj} \sqrt{\frac{2}{k_{v_{cq2}}}} \left[\frac{A_{semi}}{\sqrt{V_0 - V_{operation}} \, (l^3 A_0)^{\frac{1}{4}}} \right] \tag{21}$$

Integrating to calculate the stored charge, gives:

$$Q_{j_{cq}} = k_{cj} \sqrt{\frac{8}{k_{v_{cq2}}}} \left[\frac{A_{semi} \left(\sqrt{V_0 - V_{operation}} - \sqrt{V_0} \right)}{(l^3 A_0)^{\frac{1}{4}}} \right] \tag{22}$$

2) Constant Voltage Mode Parameterisation: Performing the same operation for the constant voltage mode generator by substituting (14) into (20) gives:

$$C_{j_{cv}} = \frac{k_{cj}}{\sqrt{k_{v_{cv3}}}} \left[\frac{A_{semi}}{\sqrt{(V_0 - V_{operation})} (l^2 A_0)^{\frac{1}{4}}} \right] \tag{23}$$

and integrating this to find the stored charge gives:

$$Q_{j_{cv}} = \frac{2 k_{cj}}{\sqrt{k_{v_{cv3}}}} \left[\frac{A_{semi} \left(\sqrt{V_0 - V_{operation}} - \sqrt{V_0} \right)}{(l^2 A_0)^{\frac{1}{4}}} \right] \tag{24}$$

C. Device Off-State Leakage Current

The last important parameter of the MOSFET switches which affects the system performance is the off-state leakage characteristic of the device, which will reduce harvester performance if leakage occurs during section B→C of Fig. 2(a) and will reduce the efficiency of any switch-mode power conversion process. The leakage current, again from [31], is given by:

$$I_{leakage} = \frac{q n_i}{\tau} \vartheta_{dep} \tag{25}$$

where n_i is the intrinsic carrier concentration in silicon, ϑ_{dep} is the depletion layer volume and τ is the carrier lifetime, taken as 10^{-6} s, which is typical for power MOSFETs [13].

The depletion layer width can be readily calculated [32] and assuming that the junction is asymmetrically doped in order to block high voltages, the volume of the resultant one-sided depletion layer is given by:

$$\vartheta_{dep} = A_{semi}\sqrt{\frac{2\epsilon_0\epsilon_r(V_0 - V_{operation})}{q}\left(\frac{1}{N_D}\right)} \qquad (26)$$

Therefore, substituting the optimal doping of (15) into (26), the leakage current I_l of the device in the off-state can be written as:

$$I_l = k_{I_l}A_{semi}\sqrt{(V_0 - V_{operation})V_B} \qquad (27)$$

where $k_{I_l} = 3.9 \times 10^{-4}$ m$^{-2} \cdot \Omega^{-1}$.

1) Constant Charge Parameterisation: The leakage current for a constant charge mode generator can therefore be found by substituting (9) into (27) to give:

$$I_{l_{cq}} = k_{I_l}\sqrt{\frac{k_{v_{cq2}}}{2}}A_{semi}\sqrt{V_0 - V_{operation}}(l^3A_0)^{\frac{1}{4}} \qquad (28)$$

2) Constant Voltage Parameterisation: The same can be done for the constant voltage mode generator by substituting (14) into (27) to give:

$$I_{l_{cv}} = k_{I_l}k_{v_{cv3}}A_{semi}\sqrt{(V_0 - V_{operation})}l^2{A_0}^{\frac{1}{4}} \qquad (29)$$

D. Inductors

The on-chip integrated inductance values that appear to be achievable are in the range of 1-10 μH [33] whereas much higher values are achievable with small discrete components. Clearly, the inductance values and series resistances that can be obtained depend on the volume allocated to the inductor and this in turn depends on the amount of system volume that is set aside for the power processing circuit. As discussed in SubSec. II-A, it is assumed here that the power processing interface circuitry occupies an additional volume equal to the swept volume of the proof mass, and that this space is allocated in its entirety to inductors (1 inductor in the constant charge case and 2 inductors in the constant voltage case which occupy half of this volume each). It is assumed that the geometric form of the inductor (for instance the Brooks coil form) says similar as the volume changes and that the window area for the winding scales with the square of length and that turns of conductor can be accommodated with a constant packing factor. Using the Brooks coil form it was found that the resistance, R_{ind} is proportional to the number of turns squared and inversely proportional to the cube root of volume whereas the inductance, L is proportional the number of turns squared and the cube root of volume. The L/R_{ind} ratio therfore becomes:

$$\frac{L}{R_{ind}} = k_{ind}{V_{ind}}^{\frac{2}{3}} \qquad (30)$$

where k_{ind} is a constant which depends on the core material and the fill factor. Based on the integrated inductors of [33] (with a volume of 1.28×10^{-8} m^3, $L = 1.2$ μH and R_{ind}=1 Ω) at 10 MHz (a typical resonant frequency for a 10 μH inductor resonating with an open microgenerator capacitance), a value of $k_{ind} = 0.23$ H$^2\cdot\Omega^{-1}\cdot$m^{-2} was estimated and was used here. There is then also a choice to be made between the value of inductance and the series resistance to make best use of the available volume. Here it has been assumed that the inductors should have a series resistance equal to the rest of the current path, *i.e.*, equal to $R_{DS_{on}}$ of the semiconductor devices. It can be noted that the final results were very insensitive to this value for inductor resistances of between 1/10 $R_{DS_{on}}$ to $R_{DS_{on}}$.

V. Coupled Electromechanical Models

Having now obtained expressions for the semiconductor device on-state resistance, off-state leakage current, junction capacitance and also the optimal generator electrode voltage as a function of generator size l and peak acceleration A_0, we are now in a position to write the equations of the coupled system models, *i.e.* models which enable the calculation of $\eta_{coupling}$ and η_{conv} for a range of values of l and A_0. The value of η_{system} can then be calculated from the product of these terms. Many of the resulting differential equations which must be solved in order to calculate the effectiveness terms cannot be solved analytically and so were solved numerically in the time domain and verified in PSpice using behavioural models.

A. Switched Constant Charge Model

1) Calculation of Coupling Effectiveness: It is assumed that the energy required to pre-charge the variable capacitor in constant charge mode is very small compared to the energy that can be generated. This energy is therefore neglected in these calculations. As previously described, the coupling effectiveness is the ratio between the energy coupled into the damper per stroke and the maximum possible coupled energy. For the constant charge mode of operation, this is:

$$\eta_{coupling} = \left(\frac{E_{coupled} - E_{pc}}{E_{opp}}\right)^2 \qquad (31)$$

where E_{opp} is the maximum achievable energy that could be stored on the open electrodes at the end of the cycle under perfect generation conditions of no charge leakage or charge sharing, $E_{coupled}$ is the actual energy given that some charge sharing and leakage occurs and E_{pc} is the pre-charge energy prodvided to prime the variable capacitor. With reference to the circuit of Fig. 4, on electrode separation, M_1 and M_2 remain off, the drain of M_2 is held at V_{supply} (L acts as a short circuit at the mechanical frequency of the generator) and so charge leakage occurs through M_1 and is also stored in the parasitic capacitance of M_1. The equation describing the voltage on the moving capacitor during electrode separation is:

$$i_l + \frac{dq_j}{dt} = -c_g\frac{dv_g}{dt} - v_g\frac{dc_g}{dt} \qquad (32)$$

where i_l is the leakage current through the reversed biased junction (28) of M_1, dq_j/dt is the current into the junction capacitance of M_1, c_g is the capacitance between the moving electrodes, which are assumed to separate sinusoidally over a time of flight of t_f, and v_g is the voltage across the moving electrodes. The initial value of v_g is given by the optimal pre-charge voltage given in (7). Eqn. (32) can then be solved numerically to find V_{end} (the actual voltage at the end of the generation stroke) by rewriting dq_j/dt as $(dq_j/dv_g \cdot dv_g/dt)$ where dq_j/dv_g is the junction capacitance given in (21). As the open electrode capacitance is known, the value of V_{end} can then be used to calculate $E_{coupled}$ which is substituted into (31) in order to calculate $\eta_{coupling}$.

2) Conversion Efficiency: In order to transfer the generated energy from the moving electrode capacitor, M_1 and M_2 act as a synchronous buck converter, but due to the very high resonant frequency of the discharge process (due to the small inductance and capacitor values achievable), the converter is assumed to operate in single-shot mode [13] rather in a more conventional mode where the inductor current is controlled using PWM. In this mode M_1 turns on until the moving electrode capacitor voltage reaches zero, at which point M_1 turns off and M_2 turns on, allowing the inductor current to free-wheel into the battery. When M_1 turns on at the start of this process, energy stored on the junction capacitance of M_1 is dissipated and the drain voltage of M_2 rises as its junction capacitance is quickly charged. This reduces the available useful energy on the generator capacitance to ${V_{end}}'$. This voltage can be calculated from a charge balance between the generator capacitance and the junction capacitance of M_2 (which is given by (22)).

The conversion efficiency can then be calculated by evaluating the losses in both sections of the energy transfer process, *i.e.* the discharge of the generator capacitor and the free-wheel stage. This is done by solving the differential equations for circuit operation in two stages and summing the Joule losses. The discharge stage circuit operation is described by:

$$\frac{d^2v_g}{dt^2} + \frac{R}{L}\frac{dv_g}{dt} + \frac{1}{LC_{var}}v_g = \frac{1}{LC_{var}}V_{supply} \qquad (33)$$

where C_{var} is the minimum generator open position capacitance, v_g is the voltage across the generator capacitor and R is the sum of the resistances in the MOSFET and the inductor. The initial conditions are $v_g(0) = {V_{end}}'$ and $dv_g/dt(0) = 0$. The free-wheel stage behaviour is described by:

$$\frac{di}{dt} + \frac{R}{L}i + \frac{V_{supply}}{L} = 0 \qquad (34)$$

where i is the inductor current, which takes an initial value given by solving (33) and substituting for i at the point where $v_g = 0$.

The useful energy which is transferred to the energy storage element is thus $1/2 \cdot {V_{end}}'^2$ minus the losses. The value of η_{conv} is the energy transferred divided by the energy on the moving capacitor at the instant before the discharge process begins, *i.e.*:

$$\eta_{conv} = \frac{\frac{1}{2}C_{min}{V_{end}}'^2 - E_{loss}}{\frac{1}{2}C_{min}{V_{end}}^2} \qquad (35)$$

where E_{loss} is the sum of the conduction losses in the capacitor discharging and the inductor current free-wheeling stages.

B. Switched Constant Voltage Mode

In the case of constant voltage operation, $\eta_{coupling}$ can be defined in a similar way as in constant charge mode. However, η_{conv} now comprises two sub efficiencies, QV cycle efficiency, $\eta_{conv_{qv}}$, and step-down conversion efficiency, $\eta_{conv_{sd}}$. The reason for the existence of these two conversion efficiencies is that during the generation cycle for constant voltage mode, even if the electrodes are operated at the voltage which gives an optimal electrical damping force, the energy that is harvested is still less than the opportunity energy because of charge leakage which occurs continuously from the high voltage source through device blocking junctions. In addition, the priming energy in constant voltage mode is no longer insignificant compared to the energy that can be generated and so charging efficiency must now be taken into account. The step-down conversion efficiency is then simply the efficiency of the step-down process as energy is transferred from the high voltage intermediate capacitance to the low voltage battery.

1) Coupling Effectiveness: As the variable capacitor is operated at constant voltage and thus at constant force throughout the generation stroke, the coupling effectiveness is simply defined as:

$$\eta_{coupling} = \left(\frac{V_{opp}}{V_{opp_{opt}}}\right)^2 \qquad (36)$$

where V_{opp} is the voltage that the capacitor is operated at and $V_{opp_{opt}}$ is the voltage that would give rise to the optimal damping force (14). The expression is squared because the force between the electrodes is proportional to the square of the operating voltage.

2) QV Cycle Efficiency: The QV cycle efficiency for the constant voltage case is defined as:

$$\eta_{conv_{qv}} = \frac{E_{harvest}}{E_{opp}} \qquad (37)$$

where E_{opp} is the maximum energy that could have been harvested per stroke at the actual operating voltage V_{opp} with no circuit losses, and $E_{harvest}$ is the energy actually harvested per stroke. E_{opp} is:

$$E_{opp} = \frac{1}{2}C_{max}{V_{opp}}^2 \qquad (38)$$

where C_{max} is the closed generator capacitance. $E_{harvest}$ is given by:

$$E_{harvest} = C_{max}{V_{opp}}^2 - E_{loss} - E_{pc} \qquad (39)$$

where E_{loss} is the energy lost in traversing the QV loop of Fig. 5 by the action of the circuit in Fig. 6. Note that in the constant voltage transducer, for a pre-charge energy of E_{pc} the

maximum amount of energy that can be harvested is E_{pc}, *i.e.* the maximum electrical energy that can be transferred from the variable capacitor during the generation stroke (B→C in Fig. 5) is $2E_{pc}$ (which is equal to $C_{max}{V_{opp}}^2$).

There are three components to E_{loss} in this QV cycle:

- Energy lost in pre-charging the capacitor
- Energy lost in reverse biasing the junction of M_2 as the capacitance reduces
- Energy loss due to leakage current in M_2

The loss associated with pre-charging C_{var} to V_{opp} in Fig. 6 can be calculated in the same way as the discharge losses were calculated for the transfer of energy from the generator capacitor to V_{supply} in the constant charge case: the differential equations for the charging and free-wheeling stages of the buck converter involving M_1 and M_2 in Fig. 6 are solved and the conduction losses can be summed.

The energy loss associated with the charge leakage is calculated by multiplying the leakage current by the operating voltage and the cycle time, to give:

$$E_{leak} = V_{opp} I_l / f \tag{40}$$

where V_{opp} is the actual operating voltage, I_l is given by substituting V_{opp} into (29) and f is the frequency of the mechanical excitation.

The energy loss associated with the reverse recovery charge of M_2 is simply given by:

$$E_{rr} = V_{opp} Q_{j_{vopp}} \tag{41}$$

where $Q_{j_{vopp}}$ is (24) evaluated at V_{opp}.

The value of η_{qv_c} can now be calculated by substituting the results of the individual loss components into (39) which is then substituted into (37).

3) Step-Down Efficiency: The step down efficiency, $\eta_{conv_{sd}}$, for the energy transfer from the intermediate capacitance into V_{supply} in Fig. 6 can be evaluated by solving the differential equations for the circuit in the two stages of energy transfer (inductor charging and free-wheeling) and by evaluating the conduction and diode reverse recovery losses that occur during this process. In the calculation of this efficiency, it is assumed that on each cycle an amount of energy is removed from the intermediate capacitor that is equal to the energy harvested, allowing the electrode voltage to remain in steady state from cycle to cycle.

VI. Simulation Method

All of the models presented here have been solved using time domain simulation in MATLAB with the optimisation, (*i.e.* finding the optimal semiconductor area, A_{semi}), being performed with a simple parameter sweep. The results from MATLAB were then checked against time domain simulations in PSpice. The values of A_{semi} were assumed to be multiples of 6.5×10^{-13} m^2, as this is the state of the art for minimum MOSFET cell area, as represented by the Vishay PowerPAK device family [34]. Cube lengths, l, of between 0.1 mm and 1 cm were investigated as this was thought to represent the useful range of generator sizes: when $l < 0.1$ mm, harvesters do not produce useful levels of power under realistic excitations, whilst the largest electrostatic generators reported to date have volumes approaching 1 cm^3. Harvester performance for acceleration levels between 0.1 mg and 10 g were investigated.

The maximum allowed electrode voltage is limited by the lower of two values: the maximum semiconductor junction blocking capability and the breakdown voltage of the dielectric between the electrodes. Commercial MOSFETs are able to block voltages of up to 1.5 kV [35]). The dielectric will be a low pressure gas (assuming the system is in a vacuum package) and the maximum breakdown voltage of gas at low pressures over small gaps is described by a modified version of Paschen's curve. Assuming that a pressure of 1 Pa can be obtained (as the state of the art in MEMS packaging [23]), extrapolating the results in [36] from 4 Pa to 1 Pa gives maximum dielectric breakdown voltages of around 4 kV over a 5 μm gap. Therefore, in both the constant charge and constant voltage cases, the semiconductor device limit is the lower and thus in the simulations a maximum electrode voltage of 1.5 kV is used.

The algorithm used to calculate the maximum value of η_{system} is as follows:

- The optimal pre-charge voltage (constant charge mode) or optimal operating voltage (constant voltage mode) is found for the given l and A_0 from (7) or (12) respectively.
- If these voltages cause the electrode voltage to exceed 1.5 kV, the pre-charge, or operating voltage is reduced so that the maximum voltage obtained is equal to 1.5 kV, thus moving away from optimality but ensuring breakdown does not occur.
- The value of η_{system} is then found for different numbers of semiconductor cells, allowing the optimal number of cells to be found and the maximum value of η_{system} to be found.

VII. Results and Discussion

A. Constant Charge Mode

A plot of η_{system} for the constant charge mode of operation for a harvester operating at 1 kHz is shown in Fig. 10. Each point on each plot shows η_{system} for a value of A_{semi} that is optimised for that specific point. As can be seen, there is a very narrow band over which the harvester can achieve effectiveness of 10% or above and the effectiveness drops away rapidly outside of that area. We can approximate two straight lines (on log-log axes) between which the effectiveness is greater than 10%, giving:

$$0.035{A_0}^{-0.88} < l < 0.22{A_0}^{-0.72} \tag{42}$$

where l is measured in mm and A_0 is measured in m/s^2. The reasons for the very poor performance under certain values of A_0 and l are:

- Small values of A_0 and l: In the right corner of Fig. 10, the reduction in system effectiveness is primarily because as microgenerator size decreases, the closed and open values of the moving electrode capacitor decrease and become comparable to the parasitic capacitances of even

the smallest practical MOSFET cells, which significantly reduces $\eta_{coupling}$ (Fig. 11) due to charge sharing. When in this low effectiveness region, an increase in l causes the generator capacitance to increase, reducing the effect of the parasitic capacitances, and an increase in A_0 increases the required pre-charge voltage, pushing the blocking junctions into a lower capacitance region, which also reduces the effect of the parasitic capacitances.

- Large values of A_0 and l: In the left corner of Fig. 10 the very low value of system effectiveness at high values of l and A_0 comes from the requirement that for the generator to operate optimally in this region the final generator voltage would exceed the 1.5 kV limit. This reduces $\eta_{coupling}$ as shown in Fig. 11. However, as can be seen from Fig. 10, the system effectiveness drops gradually as both acceleration and length increase before the very rapid reduction in $\eta_{coupling}$ occurs. This is due to a gradual reduction in η_{conv}, as highlighted in Fig. 12. The performance of the power electronic circuits decreases as the voltage blocking requirement increases, because the specific on resistance of the devices increases.

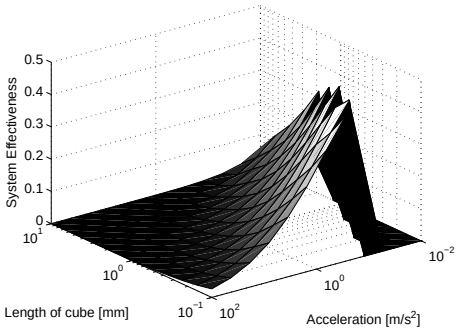


Fig. 10. Maximum effectiveness of a constant charge microgenerator operated at 1 kHz.

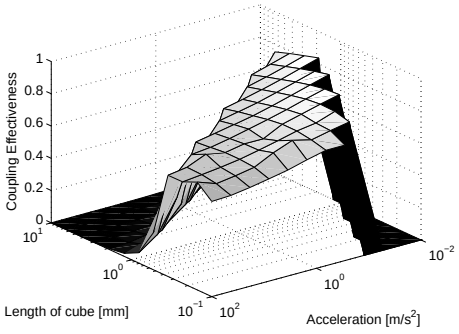


Fig. 11. Maximum coupling effectiveness of a constant charge microgenerator operated at 1 kHz.

Whilst the value of η_{system} decreases with increased values of l and A_0 (past some optimal values), the total available power output from the device does continue to increase as l is increased. The total useful power output available from this system, operated with an excitation frequency of 1 kHz is shown in Fig. 13.

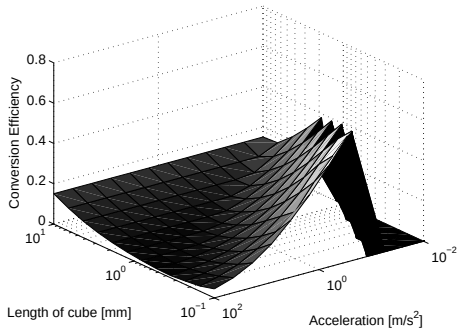


Fig. 12. Maximum conversion efficiency of a constant charge microgenerator operated at 1 kHz.

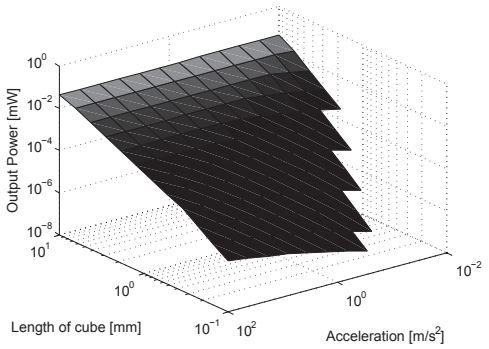


Fig. 13. Maximum useful processed output power of a constant charge microgenerator operated at 1 kHz.

Fig. 14 shows the system effectiveness of a constant charge generator at an excitation frequency of only 1 Hz. As can be seen, the general trend is the same as the high frequency operation shown in Fig. 10, although the peak performance is slightly reduced. This is because the effects of charge leakage become more apparent at low frequency. However, as the reduction in η_{system} is relatively small even as the frequency is reduced as low as 1 Hz, it can be ascertained that the reason for low effectiveness values is mainly due to charge sharing effects rather than those of charge leakage.

B. Constant Voltage Mode

Fig. 15 shows the upper limit on η_{system} for a constant voltage mode generator operated at 1 kHz. As can be seen, the useful operating envelope of the constant voltage mode of operation far exceeds that of the constant charge generator. Whilst the constant charge mode device failed to reach value of η_{system} of even 0.5, the constant voltage mode device is able to exceed this value over a reasonably wide operating envelope. In order for the generator to achieve a value of η_{system} of at least 0.5, the generator should be operated within the following bounds:

$$0.079{A_0}^{-0.20} < l < 0.0050{A_0}^{-2.5} \tag{43}$$

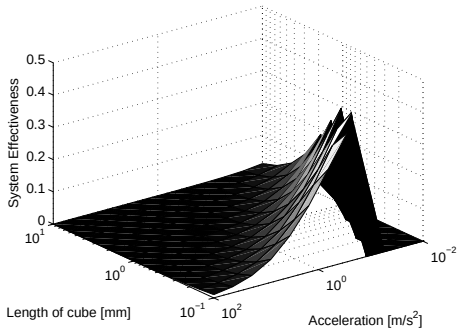


Fig. 14. Maximum effectiveness of a constant charge microgenerator operated at 1 Hz.

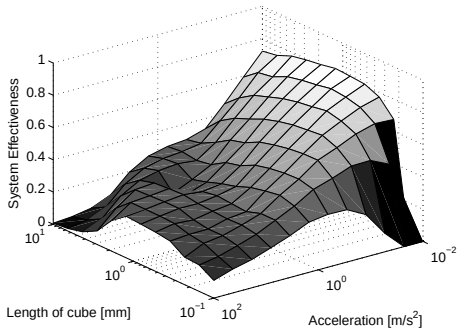


Fig. 15. Maximum effectiveness of a constant voltage microgenerator operated at 1 kHz.

Figs. 16 to 18 show the values of the constituent parts of the effectiveness and efficiency of the system which allows us to understand the reason for the system effectiveness to be low in some regions of the plot. These reasons are:

- Small values of A_0 and l: the required operating voltage to generate the optimal damping force is low and the charge required during generator priming to reverse bias the junction of M_2 (Fig. 6) becomes a larger proportion of the total supplied energy from V_{source} during the pre-charge phase as the optimal force reduces. This energy is never recovered and thus $\eta_{conv_{qv}}$ is reduced, reducing η_{system}. The limit occurs because of the limit on the minimum size of A_{semi}.
- Large values of A_0 and l: as was the case the in the constant charge mode of operation, at very high values of A_0 and l, the required optimal damping force cannot be reached because of the limit set here on semiconductor blocking voltages to 1.5 kV. The effect of this constraint can be seen in Fig. 16, where $\eta_{coupling}$ drops rapidly. However, before this point is reached, there is still a slow reduction in system effectiveness as l and A_0 increase. This is again due to the increase in specific on resistance of the devices as voltage blocking requirements increase.
- Small values of l: at small generator dimensions, the value of $\eta_{coupling}$ decreases (Fig. 16) as a non-negligable fraction of the device volume is utilised by the transduction mechanism rather than the proof mass.

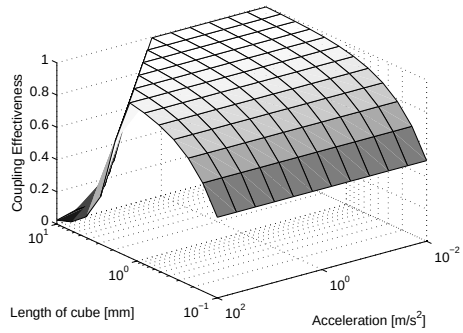


Fig. 16. Maximum coupling effectiveness of a constant voltage microgenerator operated at 1 kHz.

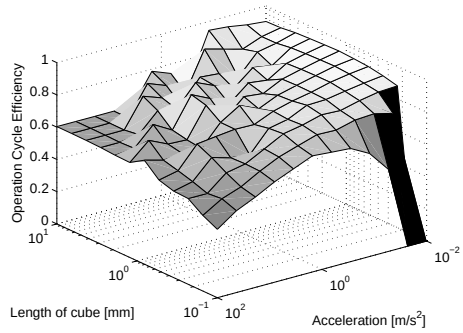


Fig. 17. Maximum QV-cycle efficiency of a constant voltage microgenerator operated at 1 kHz.

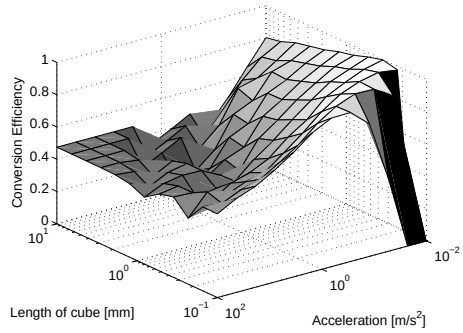


Fig. 18. Maximum step-down conversion efficiency of a constant voltage microgenerator operated at 1 kHz.

Fig. 19 shows the maximum output power from the constant voltage mode device at an excitation frequency of 1 kHz. The power outputs from this device are clearly superior to those for the constant charge device in Fig. 13.

Fig. 20 shows the system effectiveness of a constant voltage microgenerator with a mechanical excitation frequency of 1 Hz. As can be seen, at this reduced frequency, the behaviour is broadly the same as the high frequency performance, although the peak effectiveness is slightly reduced and the useful operating envelope is also reduced. The reason for the reduction in performance with frequency is the same as in the

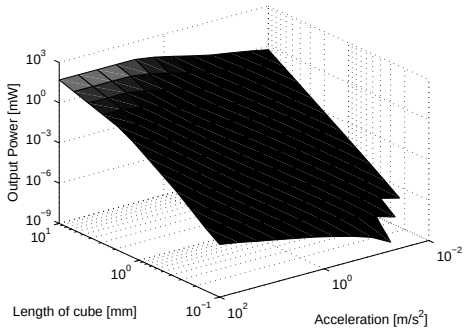


Fig. 19. Maximum power output of a constant voltage microgenerator operated at 1 kHz.

constant charge case: increased flight times of the electrodes increase the effects of leakage currents.

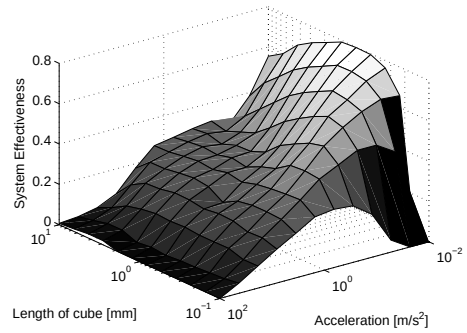


Fig. 20. Maximum effectiveness of a constant voltage microgenerator operated at 1 Hz.

VIII. Choice of Operating Mode

It is clear that when the transduction mechanism and the interface circuit are considered together as a system, even when optimised, the theoretical limits on performance of electrostatic energy harvesters is acceptable over only a relatively small operating range. The constant voltage mode configuration of generator is superior to the constant charge mode device in that it can generate with an effectiveness of over 50% over a reasonably large operating envelope, whilst the constant charge device fails to ever reach an effectiveness of 50%. This is mainly because $\eta_{coupling}$ remains closer to the optimal value with constant voltage mode because charge leakage during the generation stroke (B→C in Figs. 3 and 5) does not reduce $\eta_{coupling}$ for constant voltage mode. However, the choice of constant voltage mode over constant charge mode is still not a simple one. The circuit complexity in constant voltage mode is about twice that of constant charge mode because it requires a high voltage intermediate stage.

IX. Conclusion

In this paper, the performance of switched constant voltage and constant charge mode generators connected to interface power processing circuits has been investigated. The analysis was performed by parameterising the expressions for $\eta_{coupling}$ and η_{system} as functions of generator size l, input excitation A_0 and semiconductor device area, A_{semi}. For each combination of l and A_0, the optimal semiconductor device area A_{semi} was found, allowing the ultimate limit on electrostatic generator performance to be determined.

It was shown that a system effectiveness of up to 80% is attainable for constant voltage mode devices and up to 30% is achievable for constant charge mode devices. The operating envelope for constant voltage mode devices far exceeds that of the constant charge mode device. This result is consistent with the current trend in electrostatic harvester research where constant voltage mode devices now seem to be the most common. Both of the generator types perform poorly when both the acceleration and device size are too large or too small. For large values of acceleration, the performance decreases due to the need for higher blocking capability in the MOSFETs which in turn increases their specific on resistance and reduces the power conversion efficiency. At small accelerations (for small harvester sizes) the minimum semiconductor cell size is too large and thus the generator is swamped by the semiconductor parasitic capacitance. The use of specially designed minority carrier devices, such as miniature IGBTs or thyristors, may be beneficial in improving the effectiveness at high values of acceleration, and smaller device cell sizes could improve performance at low accelerations and generator dimensions.

The scaling laws for the electrostatic transducer are favourable as dimensions decrease when the device is operated as an actuator. The same conclusion is valid when such transducers are used as generators, until limits on size and acceleration are reached, at which point the system effectiveness of the combined electromechanical system drops due to unavoidable parasitic effects in the semiconductor devices. Inequalities were given which specify constraints on device size as a function of acceleration for both constant charge and constant voltage modes harvesters for which acceptable levels of effectiveness can be achieved.

Acknowledgments

This work was supported in part by the Engineering and Physical Sciences Research Council (EPSRC) under grant number EP/G070180/1, “Next Generation Energy-Harvesting Electronics: Holistic Approach”. The authors would like to thank G. Kondala Rao for helpful discussions and the lead author is grateful to Prof Reza Ghodssi (University of Maryland) and Prof Paul Wright (UC Berkeley) for providing peaceful environments in which to work during his sabbatical.

References

[1] D. Arnold, “Review of microscale magnetic power generation,” *Magnetics, IEEE Transactions on*, vol. 43, no. 11, pp. 3940 –3951, nov. 2007.

[2] P. D. Mitcheson, T. Sterken, C. He, M. Kiziroglou, E. M. Yeatman, and R. Puers, “Electrostatic Microgenerators,” *Measurement and Control*, vol. 41, pp. 114–119, 2008.

[3] P. D. Mitcheson, P. Miao, B. H. Stark, E. M. Yeatman, A. S. Holmes, and T. C. Green, “MEMS Electrostatic Micro-Power Generator for Low Frequency Operation,” *Sensors and Actuators, part A*, vol. 115, no. 2–3, pp. 523–529, 2004.

[4] R. Amirtharajah, S. Meninger, J. O. Mur-Miranda, A. P. Chandrakasan, and J. H. Lang, "A Micropower Programmable DSP Powered using a MEMS-based Vibration-to-Electric Energy Converter," in *Solid State Circuits, IEEE International Conference*, 2000, pp. 362–363.
[5] T. M. Kamel, R. Elfrink, M. Renaud, D. Hohlfeld, M. Goedbloed, C. de Nooijer, M. Jambunathan, and R. van Schaijk, "Modelling and Characterisation of MEMS-based Piezoelectric Harvesting Devices," *Journal of Micromechanics and Microengineering*, vol. 20, pp. 1–14, September 2010.
[6] Y. Lui, K. L. Ren, H. F. Hofmann, and Q. Zhang, "Investigation of Electrorestrictive Polymers for Energy Harvesting," *IEEE Transactions on Ultrasonics, Ferroelectrics, and Frequency Control*, vol. 52, no. 12, pp. 2411–2417, 2005.
[7] S. P. Beeby, R. N. Torah, M. J. Tudor, P. Glynne-Jones, T. O. O'Donnell, C. R. Sarah, and S. Roy, "A Micro Electromagnetic Generator for Vibration Energy Harvesting," *IOP Journal of Micromechanics and Microengineering*, vol. 17, pp. 1257–1265, June 2007.
[8] L. Wang and F. G. Yuan, "Vibration Energy Harvesting by Magnetorestrictive Material," *Smart Materials and Structures*, vol. 17, pp. 1–14, June 2008.
[9] W. S. N. Trimmer and R. Jebens, "Actuators for Microrobots," in *Robotics and Automation, 1989. Proceedings., 1989 IEEE International Conference on*, May 1989, pp. 1547–1552.
[10] P. D. Mitcheson, E. K. Reilly, T. Toh, P. K. Wright, and E. M. Yeatman, "Performance Limits of the Three MEMS Inertial Energy Generator Transduction Types," *Journal of Micromechanics and Microengineering*, vol. 17, pp. S211–S216, August 2007.
[11] R. Guillemet, P. Basset, D. Galayko, and T. Bourouina, "Combined optimization of electrical and mechanical parameters of an out-of-plane gap-closing electrostatic vibration energy harvester (veh)," in *Design Test Integration and Packaging of MEMS/MOEMS (DTIP), 2010 Symposium on*, May 2010, pp. 73 – 78.
[12] P. Chapman and P. Krein, "Smaller is better? [micromotors and electric drives]," *Industry Applications Magazine, IEEE*, vol. 9, no. 1, pp. 62 – 67, jan/feb 2003.
[13] B. H. Stark, P. D. Mitcheson, P. Miao, T. C. Green, E. M. Yeatman, and A. S. Holmes, "Converter Circuit Design, Semiconductor Device Selection and Analysis of Parasitics for Micro-Power Electrostatic Generators," *IEEE Transactions on Power Electronics*, vol. 21, pp. 27–37, 2006.
[14] T. Sterken, P. Fiorini, K. Baert, K. Puers, and G. Borghs, "An Electret-Based Electrostatic μ-Generator," in *Proceedings of the 12th International Conference on Solid State Sensors, Actuators and Microsystems (Transducers)*, Boston, USA, June 2003, pp. 1291–1294.
[15] J. Boland, H. Chao-Yuan, Y. Suzuki, and Y. C. Tai, "Micro Electret Power Generator," in *The Sixteenth IEEE Annual International Conference on MEMS*, Kyoto, Japan, January 2003, pp. 538–541.
[16] D. Miki, Y. Suzuki, and N. Kasagi, "Effect of nonlinear external circuit on electrostatic damping force of micro electret generator," in *Solid-State Sensors, Actuators and Microsystems Conference, 2009. TRANSDUCERS 2009. International*, june 2009, pp. 636 – 639.
[17] B. Yen and J. Lang, "A variable-capacitance vibration-to-electric energy harvester," *Circuits and Systems I: Regular Papers, IEEE Transactions on*, vol. 53, no. 2, pp. 288 – 295, feb. 2006.
[18] P. D. Mitcheson, E. M. Yeatman, G. K. Rao, A. S. Holmes, and T. C. Green, "Energy Harvesting for Human and Machine Motion for Wireless Electronic Devices," *Proceedings of the IEEE*, vol. 96, no. 9, pp. 1457–1486, September 2008.
[19] P. D. Mitcheson, T. C. Green, E. M. Yeatman, and A. S. Holmes, "Architectures for Vibration-Driven Micropower Generators," *IEEE/ASME Journal of Microelectromechanical Systems*, vol. 13, no. 3, pp. 429–440, June 2004.
[20] E. M. Yeatman, P. D. Mitcheson, and A. S. Holmes, "Micro-engineered devices for motion energy harvesting," in *IEEE Internatiaonal Electron Devices Meeting, 2007*, December 2007, pp. 375 –378.
[21] S. Roundy, P. K. Wright, and K. S. Pister, "Micro-Electrostatic Vibration-to-Electricity Converters," in *2002 ASME International Mechanical Engineering Congress and Exposition*, New Orleans, Louisiana, USA, November 2002.
[22] E. Halvorsen, E. R. Westby, S. Husa, A. Vohl, N. P. Østbø, V. Leonov, T. Sterken, and T. Kvisterøy, "An Electrostatic Energy Harvester with Electret Bias," in *Proceedings of Transducers 2009*, Denver, USA, June 2009, pp. 1381–1384.
[23] B. Lee, S. Seok, and K. Chun, "A study on wafer level vacuum packaging for mems devices," *Journal of Micromechanics and Microengineering*, vol. 13, no. 5, p. 663, 2003. [Online]. Available: http://stacks.iop.org/0960-1317/13/i=5/a=318
[24] G. Kondala Rao, P. D. Mitcheson, and T. C. Green, "Mixed electromechanical simulation of electrostatic microgenerator using custom-semiconductor device models," in *Proceedings of PowerMEMS 2009*, Washington DC, USA, December 2009, pp. 356–359.
[25] R. Tashiro, N. Kabei, K. Katayama, Y. Ishizuka, F. Tsuboi, and K. Tsuchiya, "Development of an Electrostatic Generator that Harnesses the Motion of a Living Body," *JSME International Journal*, vol. 43, no. 4, pp. 916–922, 2000, series C.
[26] S. Meninger, J. O. Mur-Miranda, R. Amirtharajah, A. P. Chandrakasan, and J. H. Lang, "Vibration-to-Electric Energy Conversion," *Very Large Scale Integration (VLSI) Systems, IEEE Transactions on*, vol. 9, no. 1, pp. 64–76, February 2001.
[27] S. Meninger, J. O. Mur-Miranda, R. Amirtharajah, A. Chandrakasan, and J. Lang, "Vibration-to-Electric Energy Conversion," in *Low Power Electronics and Design, 1999, International Symposium on*, August 1999, pp. 48–53.
[28] E. O. Torres and G. A. Rincon-Mora, "A 0.7- μm BiCMOS Electrostatic Energy-Harvesting System IC," *IEEE Journal of Solid state circuits*, vol. 45, no. 2, pp. 483–496, 2010.
[29] G. J. Sheu, S. M. Yang, and T. Lee, "Development of a Low Frequency Electrostatic Comb-Drive Energy Harvester Compatible to SOC Design by CMOS Process," *Sensors and Actuators A: Physical*, vol. 167, no. 1, pp. 70–76, May 2011.
[30] B. H. Stark and T. C. Green, "Comparison of SOI Power Device Structures in Power Converters for High-Voltage, Low-Charge Electrostatic Microgenerators," *IEEE Transactions on Electron Devices*, vol. 52, no. 7, pp. 1640–1648, July 2005.
[31] D. Grant and J. Gower, *Power MOSFETS: Theory and Applications*, ser. A Wiley-interscience publication. London: Wiley, 1989.
[32] K. Leaver, *Microelectronic Devices*, 2nd ed. London: Imperial College Press, 1997.
[33] J. Boggetto, Y. Lembeye, J. Ferrieux, and J. Keradec, "Copper losses in power integrated inductors on silicon," in *Industry Applications Conference, 2002. 37th IAS Annual Meeting. Conference Record of the*, vol. 2, 2002, pp. 977 – 983 vol.2.
[34] Vishay Inc., "Press release," September 2011. [Online]. Available: http://www.vishay.com/company/press/releases/2009/090909mosfets/
[35] "SFTW4N150 data sheet," STMicroelectronics, Geneva, Switzerland, July 2009.
[36] J. M. Torres and R. Dhariwal, "Electric field breakdown at micrometre seperations in air and vacuum," *Microsystem Technologies*, vol. 6, no. 1, pp. 6–10, 1999.



Paul. D Mitcheson (SM'12) received the M.Eng. degree in electrical and electronic engineering and the Ph.D. degree from Imperial College London, U.K., in 2001 and 2005 respectively. He became a lecturer (Assistant Professor) at Imperial College in 2006 and is currently a senior lecturer (Associate Professor) in the Control and Power Research Group, Electrical and Electronic Engineering Department and Imperial College London. He has research interests in energy harvesting devices, in particular the power processing requirements for harvester powered systems.



Tim C. Green received a B.Sc. (Eng) (first class honours) from Imperial College, London, UK in 1986 and a Ph.D. from Heriot-Watt University, Edinburgh, UK in 1990. Both degrees were in electrical engineering. He was a Lecturer at Heriot Watt University until 1994 and is now a Professor of Electrical Power Engineering at Imperial College London and Deputy Head of the Electrical and Electronic Engineering Department. His main research interest is in formulating the future form the electricity network to support low-carbon futures. He also pursues the power processing of micro-generation systems for energy harvesting. He leads the FlexNet consortium of 10 UK universities researching future networks. He is a Chartered Engineer in the UK.